Communication

Rapid assignment of protein side chain resonances using projection–reconstruction of (4,3)D HC(CCO)NH and intra-HC(C)NH experiments

Ling Jiang, Brian E. Coggins, Pei Zhou *

Department of Biochemistry, Duke University Medical Center, 242 Nanaline Duke Building, Research Drive, Durham, NC 27710, USA

Abstract

The reconstruction of higher-dimensional NMR spectra from projections can provide significant savings in instrument time. Here, we demonstrate its application to the (4,3)D HC(CCO)NH and intra-HC(C)NH experiments. The latter experiment contains a novel intra-residue filter element, which selectively correlates the side chain resonances with the corresponding intra-residue amide resonances. Compared to the conventional HC(C)NH experiment, the intra-HC(C)NH experiment reduces the spectral complexity and thus the minimum number of projections required for artifact-free reconstruction by half. The use of the projection–reconstruction technique allows rapid data collection and unambiguous assignment of aliphatic side chain nuclei at high resolution.
© 2005 Elsevier Inc. All rights reserved.

Keywords: Projection–reconstruction; Intra-HC(C)NH; Multidimensional NMR; Side chain assignment

1. Introduction

A prerequisite for detailed structural analyses or dynamic studies of proteins by high resolution NMR is the assignment of backbone and side chain resonances. The introduction of ^{15}N and ^{13}C labeling has made it possible to assign all of the proton and carbon resonances of the aliphatic side chains by recording HCCH–TOCSY, HC(CCO)NH, or HC(C)NH experiments using ^{13}C–^{13}C TOCSY spin locks [1–8]. Among these experiments, the latter two are particularly attractive because they correlate side chain resonances with the more dispersed backbone HN resonances. In addition, since the HC(CCO)NH experiment correlates the sequential side chain resonances and the HC(C)NH experiment correlates both the intra- and sequential side chain resonances to the backbone amides, these two experiments can also be used to assist with sequential assignment [6,7].

Due to significant overlap of side chain resonances, recording these side chain experiments in the 4D mode is particularly attractive. In this case, the chemical shifts of the aliphatic protons and their attached carbons are recorded simultaneously, allowing further separation of the signals, and also providing a basis to analyze other spectra based on the ^1H–^{13}C correlation, such as 3D ^{13}C-separated NOESY, 4D $^1H/^{13}C$ HMQC–NOESY–$^1H/^{13}C$ HMQC or 4D $^1H/^{13}C$ HMQC–NOESY–$^1H/^{15}N$ HSQC experiments [9–13]. The benefit of recording a conventional 4D spectrum, however, is hampered by the lengthy experimental time required to sample each of the four dimensions independently. Even with an extremely low digital resolution, the required measurement time is typically longer than 7–8 days. As a result, the 3D variants of such experiments, such as H(CCCO)NH and (H)C(CCO)NH, are usually utilized, with aliphatic proton and carbon resonances being

---

* Corresponding author. +1 919 684 8885.
 E-mail address: peizhou@biochem.duke.edu (P. Zhou).

recorded separately. The analysis of these 3D spectra is often complicated by signal overlap and the difficulty of assigning the correct proton resonances to their attached carbon atoms.

Recently, several groups have contributed to the development of methods utilizing simultaneous evolution of multiple dimensions to speed up data collection [14–23]. The intrinsic connection of these methodologies was initially pointed out by Coggins and collaborators [24]; their strength and weakness have recently been discussed by Kupče and Freeman in an excellent review [25]. Several algorithms have been proposed to reconstruct the original higher dimensional spectrum with a small number of projections [21,26–28]. The benefits and weaknesses of these algorithms are discussed in detail by Venters et al. [27].

With the lower-value algorithm, the number of projections needed to obtain an artifact-free spectrum can be estimated based on the number of signals in the projection space and their relative distribution [27]. Assuming that there are m well-separated peaks in the projection space, the number of projections (n) needed for an artifact-free reconstruction is determined by the following equation:

$$n \geqslant m(d - p) + 1, \tag{1}$$

where d is the number of dimensions in the reconstruction and p is the number of dimensions on the projections. For reconstruction of 4D spectra from 3D projections, provided that the side chain signals are well resolved, one would need a maximum of 10 projections to produce an artifact-free spectrum. This estimate is based on the signal distribution of the most complicated spin system, a lysine residue, containing nine potential signals. The above analysis also indicates that the HC(C)NH experiment is not well suited for the projection–reconstruction approach as the number of side chain signals is statistically doubled compared with its counterpart, the HC(CCO)NH experiment. In addition, the presence of intra- and sequential side chain resonances increases the chance of signal overlap in the spectrum. Both of these factors would require more projections, and thus longer instrument time, to reconstruct an artifact-free spectrum. The development of experiments detecting only intra-residue correlations is ideally suited to resolve this problem [29–31]. Unfortunately, all of the previously reported intra-type experiments have been designed for magnetization transfers along an "out-and-back" pathway and cannot be applied to a "walk-through" type of experiment, such as the HC(C)NH experiment. Here, we propose an intra-residue filter element for the "walk-through" type of experiments and demonstrate its application in the intra-HC(C)NH experiment. Reconstruction of high-resolution 4D HC(CCO)NH and intra-HC(C)NH spectra from 3D projections collected within 48 h allowed

complete separation of aliphatic side chain resonances, including the majority of methylene groups.

2. Results and discussion

2.1. Intra-HC(C)NH

2.1.1. Pulse sequence

The proposed intra-HC(C)NH pulse sequence (Fig. 1) was developed based on the optimized HC(C)NH pulse sequence by Lin and Wagner [4] with the addition of an intra-residue filter element. This pulse sequence correlates the chemical shifts of side chain protons to their directly attached carbons, and to the backbone N and HN within the same residue. The magnetization of side chain protons is transferred to their directly attached carbon atoms using an INEPT step, which is then transferred to the Cα by a DIPSI3 mixing scheme [32]. During the intra-residue filter element, the Cα magnetization is transferred to the nitrogen within the same residue, and then transferred to the attached amide proton for detection.

$$^{1}\text{H}_{\text{aliph}}(i)[t1] \xrightarrow{^{1}J_{\text{HC}}} {}^{13}\text{C}_{\text{aliph}}(i)[t2] \xrightarrow{\text{DIPSI3}} \text{C}\alpha(i)$$
$$\xrightarrow{^{1}J_{\text{C}\alpha\text{CO}}, ^{1}J_{\text{NC}\alpha}, ^{2}J_{\text{NC}\alpha}, ^{1}J_{\text{NCO}}} {}^{15}\text{N}(i)[t3] \xrightarrow{^{1}J_{\text{HN}}} {}^{1}\text{HN}(i)[t4]. \tag{2}$$
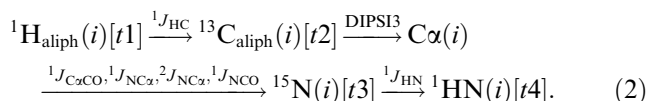
The intra-residue filter exploits the one-bond and two-bond J couplings between Cα, CO, and N ($^{1}J_{\text{C}\alpha\text{CO}}$, $^{1}J_{\text{NC}\alpha}$, $^{2}J_{\text{NC}\alpha}$, and $^{1}J_{\text{NCO}}$). Starting from $\text{C}\alpha_x^i$ (Fig. 1, point a), the anti-phase coherence $2\text{C}\alpha_y^i\text{CO}_z^i$ is generated after a delay of $2Ta$ (point b), which is then transformed to double quantum coherence $-2\text{C}\alpha_y^i\text{CO}_y^i$ by a 90° carbonyl pulse. During the $2Tc$ delay (Fig. 1, b–c), the J coupling between Cα and carbonyl is no longer active, while the J coupling between carbonyl and sequential nitrogen generates the coherence $4\text{C}\alpha_y^i\text{CO}_x^i\text{N}_z^{i+1}$ (point c). The transverse magnetization of carbonyl is flipped back to z-axis by a following 90° carbonyl pulse along y-axis, and refocused to $2\text{C}\alpha_x^i\text{N}_z^{i+1}$ by the coupling between Cα and CO during the second $2Ta$ delay (points c and d).

In addition, during the entire delay of ($4Ta + 2Tc$) of the intra-residue filter element between time points (a) and (d), the $^{1}J_{\text{NC}\alpha}$ and $^{2}J_{\text{NC}\alpha}$ couplings between Cα and the intra- and sequential nitrogen nuclei are active, which generate the coherences listed below:

$$2\text{C}\alpha_x^i\text{N}_z^{i+1} \rightarrow \left\{ \begin{array}{c} 4\text{C}\alpha_y^i\text{N}_z^i\text{N}_z^{i+1} \\ \text{C}\alpha_y^i \\ -2\text{C}\alpha_x^i\text{N}_z^i \\ 2\text{C}\alpha_x^i\text{N}_z^{i+1} \end{array} \right\}. \tag{3}$$

The 90° Cα pulse along the y-axis and the following crush gradient ($g7$) remove the coherences containing the $\text{C}\alpha_y^i$ component. The remaining two coherences
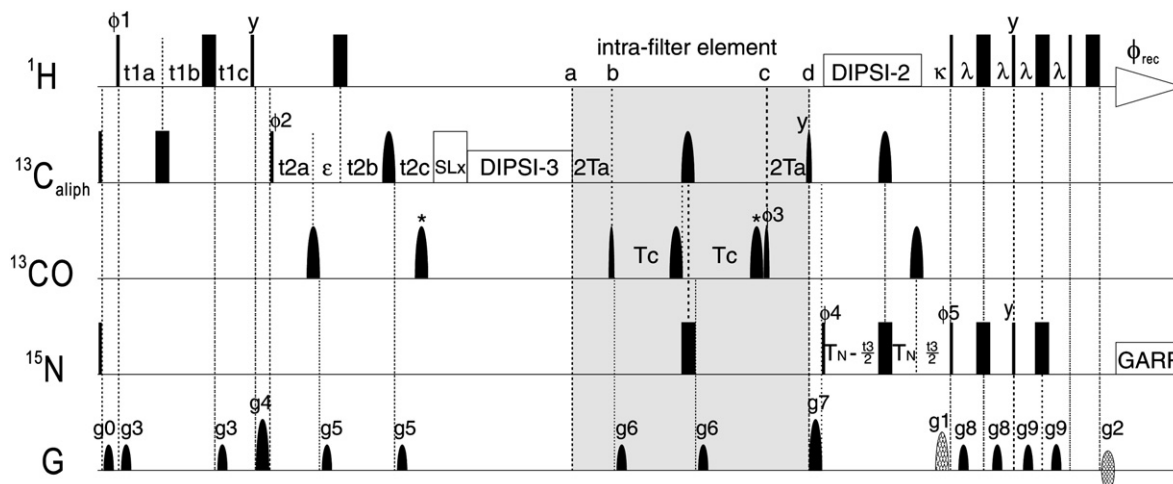
Fig. 1. Pulse scheme of the intra-HC(C)NH experiment. Narrow and wide bars or shapes represent 90° and 180° hard pulses or selective pulses, respectively. Unless indicated otherwise, pulses are applied along the x-axis. The ^{1}H carrier is set initially to 2.7 ppm and then shifted to 4.7 ppm (water) immediately after the first INEPT step and before gradient $g4$. The ^{13}C and ^{15}N carriers are centered at 43.5 and 120 ppm, respectively. On a Varian Inova 600 MHz spectrometer, the hard pulses for ^{1}H, ^{13}C, or ^{15}N are applied using field strengths of 30.5, 16.7 or 7.8 kHz, respectively. ^{1}H decoupling is achieved using a 5.4 kHz DIPSI-2 sequence centered at 4.7 ppm [32]; ^{15}N decoupling during acquisition is achieved using a 1.1 kHz GARP-1 sequence [37]. The selective 180° ^{13}C pulse on aliphatic carbons before the 0.5 ms spin lock (SL) pulse is applied at a field strength (Hz) of $\Delta/\sqrt{3}$, where Δ is the separation in Hertz between the centers of the aliphatic carbons (43.5 ppm) and CO (174 ppm). The RF field for DIPSI3 mixing is 9.3 kHz [32]. Selective ^{13}Cα (centered at 56 ppm) or ^{13}CO (centered at 174 ppm) pulses used after DIPSI3 are applied as phase modulated rectangular or sinc pulses since the carbon carrier is centered at 43.5 ppm [32]. All of the selective ^{13}Cα or ^{13}CO pulses are applied with field strengths of 4.7 kHz (90° Cα), 10.5 kHz (180° Cα), 5.3 kHz (90° CO), or 11.8 kHz (180° CO), respectively, so that the application of Cα pulses has minimal excitation on CO and vice versa. The positions of the Bloch–Siegert compensation pulses are indicated by asterisks above the pulses. The off-resonance effect caused by the 180° Cα pulse during the intra-residue filter element between points b and c is compensated by the addition of an appropriate small phase correction to $\phi3$. The phase cycle is $\phi1 = (x)$; $\phi2 = (x, -x)$; $\phi3 = (y)$; $\phi4 = (x)$; $\phi5 = (x)$; $\phi_{rec} = (x, -x)$. Quadrature detections in F1 and F2 are achieved via States-TPPI of $\phi1$ and $\phi2$ [38]. Quadrature detection in F3 is achieved using sensitivity enhanced gradient scheme by alternating the signs of $g2$ and $\phi5$ [39]. The delays used in the sequence are: $T_{CH} = 1.7$ ms, $\varepsilon = 1.05$ ms, $Ta = 4.5$ ms, $Tc = 18.5$ ms, $T_N = 14.0$ ms, $\kappa = 5.4$ ms, $\lambda = 2.4$ ms. During $t1$ evolution time, $t1a = t1/2 + T_{CH}$, $t1b = t1/2 - \xi_1$, $t1c = T_{CH} - \xi_1$, where ξ_1 is a hyperbolic function defined by: $\xi_1 = T_{CH}$ for $t1 = 4T_{CH}$, $\xi_1 = 1/(2/t1 + 1/2T_{CH})$ for $t1 < 4T_{CH} < AT$ (total acquisition time), $\xi_1 = 1/(2/t1 + 1/T_{CH} - 2/AT)$ for $2T_{CH} \leqslant AT < 4T_{CH}$, and $\xi_1 = t1/2$ for $AT < 2T_{CH}$. Note this is similar to the hyperbolic function described by Lin and Wagner [4] except ξ_1 is set to $t1/2$ when total acquisition time is less than $2T_{CH}$ to avoid a negative delay for $t1b$. The same semi-constant approach is used during $t2$ evolution where the $t2a$, $t2b$, and $t2c$ are defined by $t2a = t2/2$, $t2b = t2/2 - \xi_2$, $t2c = \varepsilon - \xi_2$, with ξ_2 defined similarly to ξ_1 except that T_{CH} is replaced by ε. The durations and strengths of the gradients are: $g0 = (1$ ms, 11.10 G/cm), $g1 = (2$ ms, 22.19 G/cm), $g2 = (0.2$ ms, 22.19 G/cm), $g3 = (0.25$ ms, 5.10 G/cm), $g4 = (1$ ms, 25.07 G/cm), $g5 = (0.25$ ms, 4.37 G/cm), $g6 = (0.5$ ms, 21.52 G/cm), $g7 = (1$ ms, 21.52 G/cm), $g8 = (0.9$ ms, 19.30 G/cm), $g9 = (0.9$ ms, 16.20 G/cm).

represent the intra- and sequential correlations between Cα and nitrogen with different coefficients. In addition, the signal intensity is modulated by the passive J-coupling between Cα and Cβ. As a result, the transfer amplitudes of intra- and sequential residue coherence are modulated by:

$$I_{intra} \propto \sin(\pi^1 J_{NC\alpha}(4Ta + 2Tc))\sin(\pi^2 J_{NC\alpha}(4Ta + 2Tc))$$
$$\sin^2(\pi^1 J_{C\alpha CO}(2Ta))\sin(\pi^1 J_{NCO}(2Tc))\cos(\pi^1 J_{C\alpha C\beta}(4Ta + 2Tc)),$$
$$I_{seq} \propto \cos(\pi^1 J_{NC\alpha}(4Ta + 2Tc))\cos(\pi^2 J_{NC\alpha}(4Ta + 2Tc))$$
$$\sin^2(\pi^1 J_{C\alpha CO}(2Ta))\sin(\pi^1 J_{NCO}(2Tc))\cos(\pi^1 J_{C\alpha C\beta}(4Ta + 2Tc)).$$
$$(4)$$

Typically, $^1 J_{C\alpha CO}$ and $^1 J_{NCO}$ are 55 and 15 Hz, respectively. To maximize the intra-residue signals, Ta is set to 4.5 ms ($\sim 1/4^1 J_{C\alpha\,CO}$). Tc is optimized to be 18.5 ms for protein G B1 domain at 37 °C. If Cβ decoupling is implemented, a shorter delay (~ 15 ms) can be used [33]. The $^1 J_{NC\alpha}$ and $^2 J_{NC\alpha}$ coupling constants vary

slightly depending on the local secondary structure, hydrogen bonding and other factors in the protein. For average values measured for $^1 J_{NC\alpha}$ and $^2 J_{NC\alpha}$ in α-helices (9.6 and 6.4 Hz, respectively), β-sheets (10.9 and 8.3 Hz, respectively), or random coils (10.6 and 7.5 Hz, respectively) [34], based on Eq. (4), the coefficient for intra-residue transfer (I_{intra}) is calculated to be 0.89 for α-helices, 0.94 for β-sheets, or 0.93 for random coils; while the coefficient for sequential transfer (I_{seq}) is −0.04 for α-helices, −0.04 for β-sheets, or −0.07 for random coils (Fig. 2E). Thus the relative intensities of intra-residue signals are at least 10-fold larger than their sequential counterparts. In practice, no sequential connectivity has been observed.

2.1.2. Comparison with HC(C)NH and HC(CCO)NH

To demonstrate the performance of the intra-HC(C)NH experiment, we have collected 2D ^{13}C–^{1}HN orthogonal projections of the intra-HC(C)NH,
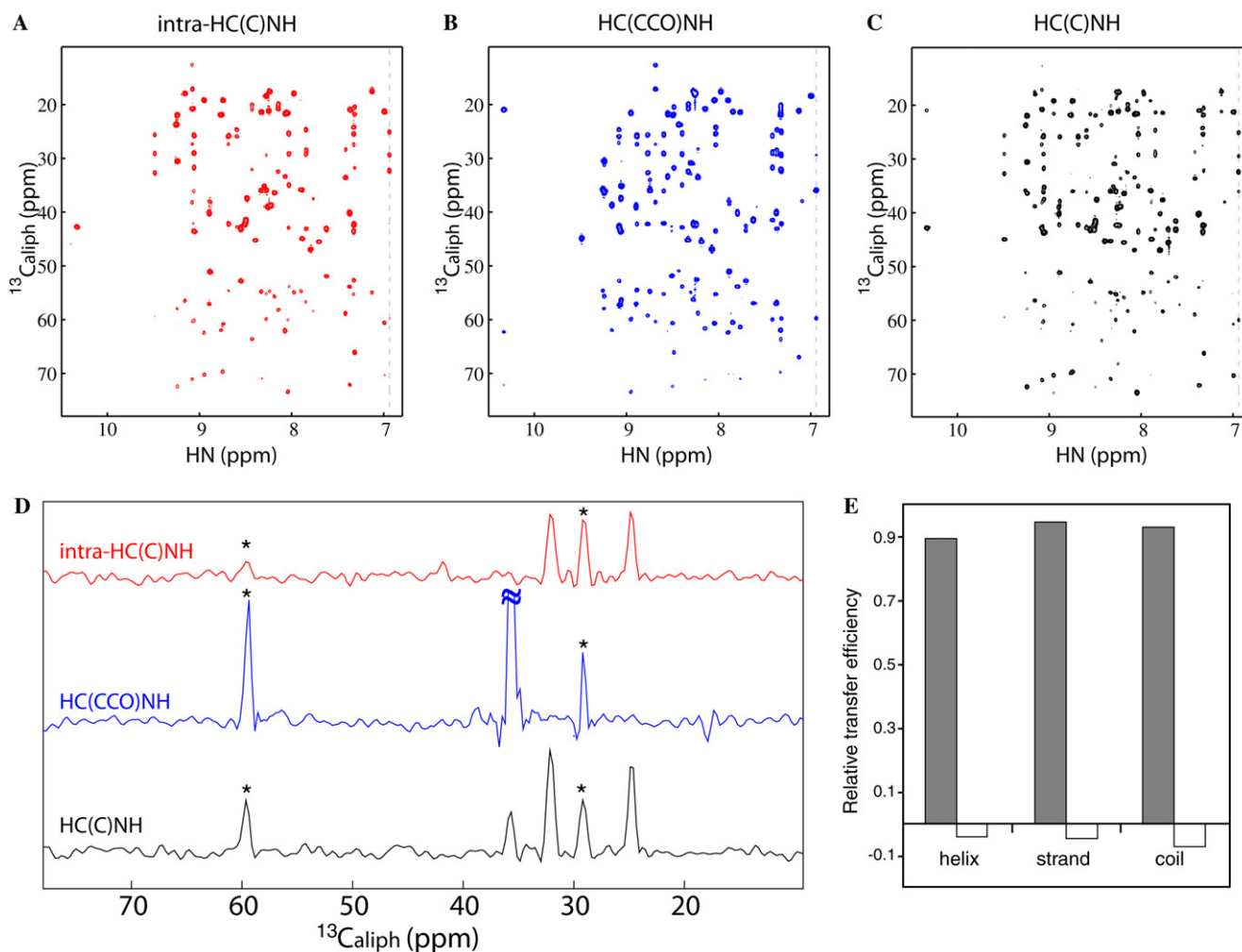
Fig. 2. 2D $^{13}C_{aliph}$–^{1}HN orthogonal planes of the 4D intra-HC(C)NH (red), 4D HC(CCO)NH (blue), and 4D HC(C)NH (black) spectra of G B1 domain on 600 ^{1}H MHz at 37 °C. The intra-HC(C)NH spectrum was recorded using the pulse sequence in Fig. 1. The HC(CCO)NH and HC(C)NH spectra were recorded using the corresponding 3D pulse sequences by Lin and Wagner [4]. (D) 1D $^{13}C_{aliph}$ traces extracted from the 2D planes along the dashed lines, from the intra-HC(C)NH (red), HC(CCO)NH (blue), and HC(C)NH (black), respectively. The peaks marked by asterisks are overlapped resonances from E27 and K28. The relative transfer efficiencies of intra- (gray bars) and sequential (white bars) side chain resonances in the intra-HC(C)NH experiment are calculated for different secondary structural regions using the average $^{1}J_{NC\alpha}$ and $^{2}J_{NC\alpha}$ values of (9.6 Hz, 6.4 Hz) for α-helix, (10.9 Hz, 8.3 Hz) for β-strand and (10.6 Hz, 7.5 Hz) for random coil, respectively [34]. (For interpretation of the references to colour in this figure legend, the reader is referred to the web version of this paper.)

HC(CCO)NH, and HC(C)NH experiments using a 1.0 mM $^{15}N/^{13}C$ labeled protein G B1 domain, a 56-residue protein at 37 °C on a Varian INOVA 600 MHz NMR spectrometer equipped with a triple-resonance cryoprobe. The NMR buffer contained 20 mM potassium phosphate, pH 6.5, 100 mM KCl and 10% D_2O. The results are shown in Figs. 2 (A–C). 1D ^{13}C traces extracted from an isolated spin system from each experiment along the dashed lines were plotted in panel (D) of Fig. 2. The prominent feature of the intra-HC(C)NH experiment is the elimination of the resonances from the preceding aliphatic side chains, which are clearly visible in the HC(C)NH spectra. As a result, the number of observed signals in the intra-HC(C)NH experiment is statistically half of those in the HC(C)NH experiment. The resulting reduction in signal overlaps is seen clearly

in the 1D traces in Fig. 2D, where the peaks marked by asterisks are overlapped resonances from E27 and K28.

Compared to the HC(C)NH experiment, the relative sensitivity of the intra-HC(C)NH experiment is influenced by the transfer efficiency from $2C\alpha_x^i N_z^{i+1}$ to $-2C\alpha_x^i N_z^i$ modulated by $\sin(\pi^1J_{NC\alpha}$ $(4Ta + 2Tc))$-$\sin(\pi^2J_{NC\alpha}$ $(4Ta + 2Tc))$ and the transverse relaxation of CO and Cα magnetizations during the intra-residue filter element. On average, the transfer coefficient in the intra-HC(C)NH experiment is 52% larger than the corresponding coefficient from $C\alpha_x^i$ to $2C\alpha_y^i N_z^i$ in the HC(C)NH experiment (0.92 vs. 0.60). This gain in transfer efficiency partially compensates the signal loss (<43% for small- to medium-sized proteins) caused by the carbonyl transverse relaxation during the 2Tc delay. Additionally, the sensitivity of the intra-HC(C)NH

experiment is influenced by the transverse relaxation of Cα during the 55 ms delay in the intra-residue filter element. When recorded using protein G B1 domain at 37 °C, the sensitivity of the intra-HC(C)NH is 70–80% of that of HC(C)NH experiment (Fig. 2D). This modest loss in sensitivity is largely offset by the use of a cryogenic probe and the recording of the tilted spectra in 3D mode, which have provided a sufficient signal-to-noise ratio for the reconstruction of the 4D spectra using only two scans per increment. When applied to proteins with molecular weights in the range of $\sim$15 kDa ($\tau_c = \sim$8 ns), as much as 69% of the signal can be lost due to the rapid T2 relaxation of Cα magnetization. Under this circumstance, the intra-HC(C)NH experiment should benefit enormously from partial deuteration, as the relaxation rate of deuterated ^{13}Cα nuclei is approximately 7.5-fold slower than their protonated counterparts [35]. Taking into account the transfer efficiency of the relevant magnetization and the carbonyl and Cα relaxation, the overall sensitivity of the intra-HC(C)NH experiment is $\sim$74% of the HC(C)NH experiment for medium-sized proteins ($\sim$15 kDa) with fractional deuteration. The same pulse sequence in Fig. 1 can be used in this case except that deuterium decoupling is needed wherever the ^{1}H$_{aliph}$ or ^{13}C$_{aliph}$ magnetization is in the transverse plane (before point d).

2.2. Projection–reconstruction of (4,3)D HC(CCO)NH and intra-HC(C)NH

The projection of (4,3)D HC(CCO)NH and intra-HC(C)NH experiments was achieved by co-evolving aliphatic protons and their attached carbon atoms as described [24]. Ten projections at 0°, ±18°, ±36°, ±54°, ±72°, and 90° with respect to the ^{1}H$_{aliph}$ axis were collected, with a total instrument time of 47.5 h. Forty-eight, 32, and 512 complex points were collected for the tilted (^{1}H$_{aliph}$/^{13}C$_{aliph}$), ^{15}N, and ^{1}HN dimensions, respectively. Because projection experiments involve the simultaneous evolution of several dimensions, maintaining identical phase information for all of the co-evolving dimensions is critical for the reconstruction algorithm to function properly. This can be achieved by setting the initial delays for all of the co-evolving dimensions to zero so that no correction is needed for the constant and linear phases for the tilted dimension. A truncated hyperbolic function for the semi-constant time delay was used for the tilted (^{1}H$_{aliph}$ and ^{13}C$_{aliph}$) dimension to avoid a negative delay caused by extremely small increments when the projection angle is close to 0° or 90°.

The data points of the ^{15}N dimension were doubled by mirror-image linear prediction, and the data points in the tilted dimension were extended to 128 complex points by forward–backward linear prediction [36]. A 70° shifted sine-bell window function was applied in the directly observed HN dimension and a 90° shifted sine-bell window function in the tilted or ^{15}N dimension. All of the 3D data were zero-filled and Fourier transformed to yield a $256 \times 128 \times 512$ matrix. A generalized lower-value algorithm, implemented in a program (PR-CALC) to be described elsewhere, was used to reconstruct the corresponding 4D spectra from 10 3D projections without artifacts [24]. The sensitivity of the reconstructed 4D spectra is limited by the signal-to-noise ratio of individual 3D projections collected in 4.75 h. A un-
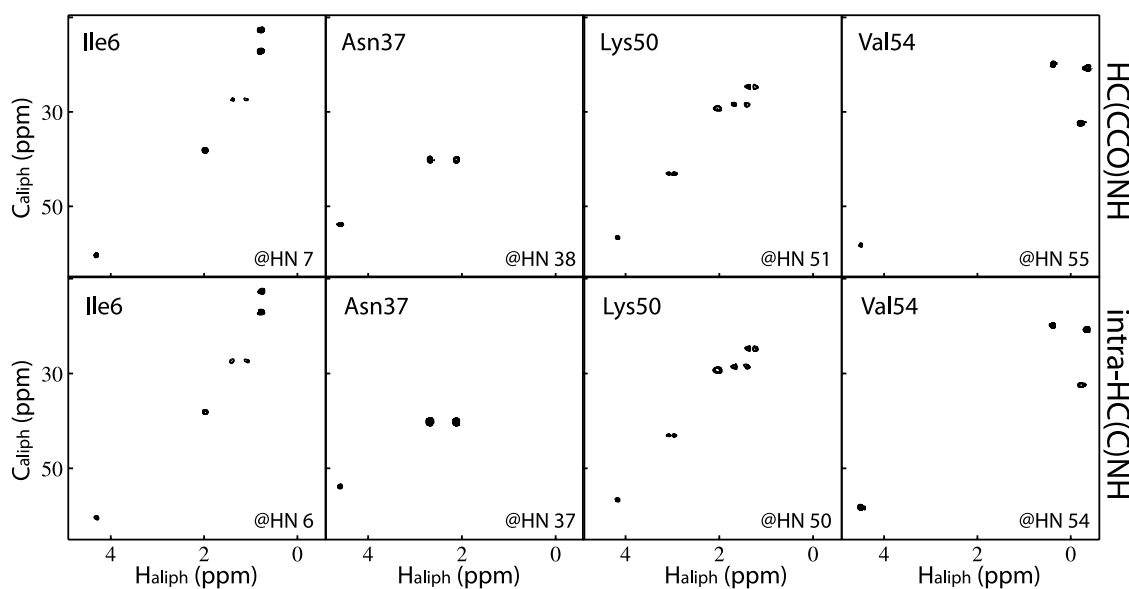
Fig. 3. Selective 2D ^{1}H$_{aliph}$–^{13}C$_{aliph}$ planes from 4D HC(CCO)NH (upper row) and intra-HC(C)NH (lower row) spectra reconstructed by a generalized lower-value algorithm. The excellent digital resolution allows complete separation of the methylene groups.

ique feature of the generalized lower-value algorithm is the capability to determine the value of each point without prior knowledge of the remaining data points in the matrix. This allowed us to build specific 2D $^1H_{aliph}$–$^{13}C_{aliph}$ planes at high-resolution for residues of interest with the corresponding nitrogen and amide proton chemical shifts derived from the ^1H–^{15}N HSQC spectrum. Slices from 4D intra-HC(C)NH and HC(CCO)NH spectra are shown in Fig. 3, illustrating the high resolution of such spectra. Since intra-HC(C)NH provides the $^1H_{aliph}$–$^{13}C_{aliph}$ correlation of side chain resonances within the same residue and HC(CCO)NH provides those of the preceding residue, the reconstructed spectra for the side chain proton–carbon correlations are identical for these two experiments except that the registration with respect to N and HN is offset by one. These spectra allowed the unambiguous correlation of the complete aliphatic side chain protons and their attached carbon nuclei. Collected using approximately 1/9th of the instrument time of the corresponding 4D spectra, these projection–reconstruction spectra provided excellent digital resolution, allowing complete differentiation for the majority of the aliphatic methylene resonances.

In summary, we report the development of an intra-HC(C)NH experiment with reduced spectral complexity compared to the HC(C)NH experiment; we further demonstrate the use of projection–reconstruction HC(CCO)NH and intra-HC(C)NH experiments for rapid data collection and unambiguous correlation of side chain aliphatic resonances. These experiments should be widely applicable to small- and medium-sized proteins for which sensitivity is not a limiting factor.

Acknowledgments

References

[1] A. Bax, G.M. Clore, A.M. Gronenborn, ^1H–^1H correlation via isotropic mixing of ^{13}C magnetization, a new three-dimensional approach for assigning ^1H and ^{13}C spectra of ^{13}C enriched proteins, J. Magn. Reson. 88 (1990) 425–431.

[2] L.E. Kay, G.Y. Xu, A.U. Singer, D.R. Muhandiram, J.D. Forman-Kay, A gradient-enhanced HCCH–TOCSY experiment for recording side-chain ^1H and ^{13}C correlations in H_2O samples of proteins, J. Magn. Reson. B 101 (1993) 333–337.

[3] G.T. Montelione, B.A. Lyons, S.D. Emerson, M. Tashiro, An efficient triple resonance experiment using carbon-13 isotropic mixing for determining sequence-specific resonance assignments

of isotopically enriched proteins, J. Am. Chem. Soc. 114 (1992) 10974–10975.

[4] Y. Lin, G. Wagner, Efficient side-chain and backbone assignment in large proteins: application to tGCN5, J. Biomol. NMR 15 (1999) 227–239.

[5] S. Grzesiek, J. Anglister, A. Bax, Correlation of backbone amide and aliphatic side-chain resonances in ^{13}C/^{15}N-enriched proteins by isotropic mixing of ^{13}C magnetization, J. Magn. Reson. B 101 (1993) 114–119.

[6] T.M. Logan, E.T. Olejniczak, R.X. Xu, S.W. Fesik, Side chain and backbone assignments in isotopically labeled proteins from two heteronuclear triple resonance experiments, FEBS Lett. 314 (1992) 413–418.

[7] B.A. Lyons, M. Tashiro, L. Cedergren, B. Nilsson, G.T. Montelione, An improved strategy for determining resonance assignments for isotopically enriched proteins and its application to an engineered domain of staphylococcal protein A, Biochemistry 32 (1993) 7839–7845.

[8] B.A. Lyons, G.T. Montelione, An HCCNH triple-resonances experiment using carbon-13 isotropic mixing for correlating backbone amide and side-chain aliphatic resonances in isotropically enriched proteins, J. Magn. Reson. B 101 (1993) 206–209.

[9] S.W. Fesik, E.R.P. Zuiderweg, Heteronuclear three-dimensional NMR spectroscopy. A strategy for the simplification of homonuclear two-dimensional NMR spectra, J. Magn. Reson. 78 (1988) 588–593.

[10] E.R.P. Zuiderweg, A.M. Petros, S.W. Fesik, E.T. Olejniczak, Four-dimensional [^{13}C, ^1H, ^{13}C, ^1H] HMQC–NOE–HMQC NMR spectroscopy: resolving tertiary nuclear overhauser effect distance constraints in the spectra of larger proteins, J. Am. Chem. Soc. 113 (1991) 370–372.

[11] G.M. Clore, L.E. Kay, A. Bax, A.M. Gronenborn, Four-dimensional ^{13}C/^{13}C-edited nuclear Overhauser enhancement spectroscopy of a protein in solution: application to interleukin 1 beta, Biochemistry 30 (1991) 12–18.

[12] G.W. Vuister, G.M. Clore, A.M. Gronenborn, R. Powers, D.S. Garrett, R. Tschudin, A. Bax, Increased resolution and improved spectral quality in four-dimensional ^{13}C/^{13}C-separated HMQC–NOESY–HMQC spectra using pulsed field gradients, J. Magn. Reson. B 101 (1993) 210–213.

[13] L.E. Kay, G.M. Clore, A. Bax, A.M. Gronenborn, Four-dimensional heteronuclear triple-resonance NMR spectroscopy of interleukin-1 beta in solution, Science 249 (1990) 411–414.

[14] T. Szyperski, G. Wider, J.H. Bushweller, K. Wüthrich, Reduced dimensionality in triple-resonance NMR experiments, J. Am. Chem. Soc. 115 (1993) 9307–9308.

[15] B. Brutscher, J.P. Simorre, M.S. Caffrey, D. Marion, Design of a complete set of two-dimensional triple-resonance experiments for assigning labeled proteins, J. Magn. Reson. B 105 (1994) 77–82.

[16] T. Szyperski, D.C. Yeh, D.K. Sukumaran, H.N. Moseley, G.T. Montelione, Reduced-dimensionality NMR spectroscopy for high-throughput protein resonance assignment, Proc. Natl. Acad. Sci. USA 99 (2002) 8009–8014.

[17] K. Ding, A.M. Gronenborn, Novel 2D triple-resonance NMR experiments for sequential resonance assignments of proteins, J. Magn. Reson. 156 (2002) 262–268.

[18] W. Kozminski, I. Zhukov, Multiple quadrature detection in reduced dimensionality experiments, J. Biomol. NMR 26 (2003) 157–166.

[19] B. Bersch, E. Rossy, J. Coves, B. Brutscher, Optimized set of two-dimensional experiments for fast sequential assignment, secondary structure determination, and backbone fold validation of ^{13}C/^{15}N-labelled proteins, J. Biomol. NMR 27 (2003) 57–67.

[20] S. Kim, T. Szyperski, GFT NMR, a new approach to rapidly obtain precise high-dimensional NMR spectral information, J. Am. Chem. Soc. 125 (2003) 1385–1393.

[21] E. Kupče, R. Freeman, Reconstruction of the three-dimensional NMR spectrum of a protein from a set of plane projections, J. Biomol. NMR 27 (2003) 383–387.

[22] E. Kupče, R. Freeman, Projection–reconstruction technique for speeding up multidimensional NMR spectroscopy, J. Am. Chem. Soc. 126 (2004) 6429–6440.

[23] B. Brutscher, DEPT spectral editing in HCCONH-type experiments. Application to fast protein backbone and side chain assignment, J. Magn. Reson. 167 (2004) 178–184.

[24] B.E. Coggins, R.A. Venters, P. Zhou, Generalized reconstruction of n-D NMR spectra from multiple projections: application to the 5-D HACACONH spectrum of protein G B1 domain, J. Am. Chem. Soc. 126 (2004) 1000–1001.

[25] R. Freeman, E. Kupče, Distant echoes of the accordion: reduced dimensionality, GFT-NMR, and projection–reconstruction of multidimensional spectra, Concepts Magn. Reson. A 23 (2004) 63–75.

[26] E. Kupče, R. Freeman, The Radon transform: a new scheme for fast multidimensional NMR, Concepts Magn. Reson. A 22 (2004) 4–11.

[27] R.A. Venters, B.E. Coggins, D. Kojetin, J. Cavanagh, P. Zhou, (4,2)D projection–reconstruction experiments for protein backbone assignment: application to human carbonic anhydrase II and calbindin D_{28K}, submitted.

[28] E. Kupče, R. Freeman, Fast multidimensional NMR: radial sampling of evolution space, J. Magn. Reson. 173 (2005) 317–321.

[29] B. Brutscher, Intraresidue HNCA and COHNCA experiments for protein backbone resonance assignment, J. Magn. Reson. 156 (2002) 155–159.

[30] D. Nietlispach, Y. Ito, E.D. Laue, A novel approach for the sequential backbone assignment of larger proteins: selective intra-HNCA and DQ-HNCA, J. Am. Chem. Soc. 124 (2002) 11199–11207.

[31] P. Permi, Intraresidual HNCA: an experiment for correlating only intraresidual backbone resonances, J. Biomol. NMR 23 (2002) 201–209.

[32] A.J. Shaka, C.J. Lee, A. Pines, Iterative schemes for bilinear operators: application to spin decoupling, J. Magn. Reson. 77 (1988) 274–293.

[33] H. Matsuo, E. Kupče, H. Li, G. Wagner, Increased sensitivity in HNCA and HN(CO)CA experiments by selective Cβ decoupling, J. Magn. Reson. B 113 (1996) 91–96.

[34] F. Delaglio, D.A. Torchia, A. Bax, Measurement of ^{15}N–^{13}C J couplings in staphylococcal nuclease, J. Biomol. NMR 1 (1991) 439–446.

[35] R.A. Venters, B.T. Farmer II, C.A. Fierke, L.D. Spicer, Characterizing the use of perdeuteration in NMR studies of large proteins: ^{13}C, ^{15}N and ^{1}H assignments of human carbonic anhydrase II, J. Mol. Biol. 264 (1996) 1101–1116.

[36] G. Zhu, A. Bax, Improved linear prediction of damped NMR signals using modified "forward–backward" linear prediction, J. Magn. Reson. 100 (1992) 202–207.

[37] A.J. Shaka, P.B. Barker, R. Freeman, Computer-optimized decoupling scheme for wideband applications and low-level operation, J. Magn. Reson. 64 (1985) 547–552.

[38] D. Marion, M. Ikura, R. Tschudin, A. Bax, Rapid recording of 2D NMR spectra without phase cycling. Application to the study of hydrogen exchange in proteins, J. Magn. Reson. 85 (1989) 393–399.

[39] L.E. Kay, P. Keifer, T. Saarinen, Pure absorption gradient enhanced heteronuclear single quantum correlation spectroscopy with improved sensitivity, J. Am. Chem. Soc. 114 (1992) 10663–10665.